

**Mesolayer of attached eddies in turbulent channel flow**

Yongyun Hwang\*

*Department of Aeronautics, Imperial College London, South Kensington, London SW7 2AZ, United Kingdom*

(Received 25 May 2016; published 4 October 2016)

Recent experimental measurements have reported that the outer peak of the streamwise wave-number spectra of the streamwise velocity depends on the Reynolds number. Starting from this puzzling observation, here it is proposed that the wall-parallel velocity components of each of the energy-containing motions in the form of Townsend's attached eddies exhibit an inner-scaling nature in the region close to the wall. Some compelling evidence on this proposition has been presented with a careful inspection of scaling of velocity spectra from direct numerical simulations, a linear analysis with an eddy viscosity, and the recently computed statistical structure of the self-similar energy-containing motions in the logarithmic region. This observation suggests that the viscous wall effect would not be negligible at least below the peak wall-normal location of each of the energy-containing motions in the logarithmic and outer regions, reminiscent of the concept of the mesolayer previously observed in the mean momentum balance. It is shown that this behavior emerges due to a minimal form of scale interaction, modeled by the eddy viscosity in the linear theory, and enables one to explain the Reynolds-number-dependent behavior of the outer peak as well as the near-wall penetration of the large-scale outer structures in a consistent manner. Incorporation of this viscous wall effect to Townsend's attached eddies, which were originally built with an inviscid approximation at the wall, also reveals that the self-similarity of the wall-parallel velocity components of the energy-containing motions would be theoretically broken in the region close to the wall.

DOI: [10.1103/PhysRevFluids.1.064401](https://doi.org/10.1103/PhysRevFluids.1.064401)**I. INTRODUCTION**

Experimental measurements and numerical simulations of wall-bounded turbulent shear flows at high Reynolds numbers over the past decade revealed that the streamwise wave-number spectra of the streamwise velocity contain an energetic peak in the logarithmic and outer regions (e.g., Refs. [1–3]). Recently, the wall-normal location of the outer peak has been reported to exhibit dependence on the friction Reynolds number  $Re_\tau$ . The wall-normal peak location  $y_{\text{peak}}$  in turbulent boundary layer was shown to be  $y_{\text{peak}}^+ \sim Re_\tau^{1/2}$  [4,5]. In the case of turbulent pipe flow, the Superpipe data seem to support the same scaling at least up to  $Re_\tau \simeq 2 \times 10^4$  [6], although a measurement from the same facility in a much wider range of Reynolds number up to  $Re_\tau \simeq 10^5$  revealed  $y_{\text{peak}}^+ \sim Re_\tau^{2/3}$  [7]. The Reynolds-number-dependent behavior of the outer peak is reminiscent of several early works which introduced the mesolayer for construction of the mean velocity [8–12]. The concept of the mesolayer relies on the observation that the inner-scaled peak wall-normal location of the Reynolds shear stress scales as  $Re_\tau^{1/2}$  [8,11,12], and the presence of such an intermediate scale between the inner and outer scales implies that the viscous wall effect on the mean velocity would not be negligible at least below the peak wall-normal location of the Reynolds shear stress [12].

Given the fact that the outer peak in the spectra of the streamwise velocity would probably indicate the long streaky motion in the outer region [i.e., very-large-scale motion (VLSM)], the emergence of its Reynolds-number-dependent behavior is quite intriguing, as it suggests that the large-scale

\*y.hwang@imperial.ac.uk

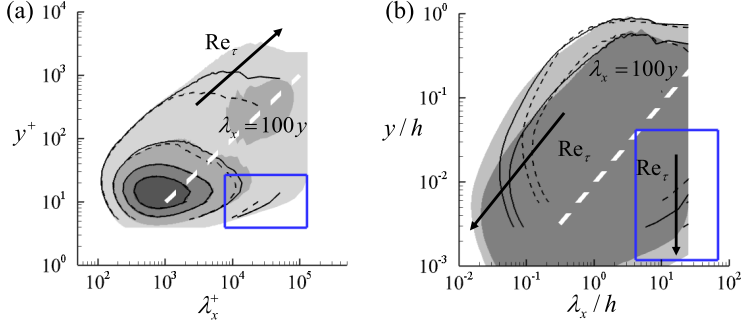


FIG. 1. Premultiplied streamwise wave-number spectra of the streamwise velocity (a) in the  $\lambda_x^+ - y^+$  plane and (b) in the  $\lambda_x/h - y/h$  plane. The contour labels in panel (a) are 0.2, 0.4, 0.6, and 0.8 times of each maximum, while those in panel (b) are 0.1 and 0.2 times of each maximum. Here, the dashed, solid, and shaded contours are respectively from  $\text{Re}_\tau = 934$ ,  $\text{Re}_\tau = 2003$  [19], and  $\text{Re}_\tau = 5186$  [3]. In each case, the region of interest is highlighted with a box.

outer structure, especially the part below the outer peak, would be under some viscous influence of the wall. In relation to this, it is interesting to remember the recent findings on the influence of the large-scale outer structure to the motions in the near-wall region [2,4,13–17]. We note that the existence of such an inner-outer interaction in the near-wall region would only be possible if the large-scale outer structure reaches the near-wall region at least to some extent (i.e., the footprint of the large-scale structure). Since the wall-normal extent of the near-wall region (say  $y^+ \simeq 50$  from Ref. [18]) in the outer unit becomes small on increasing Reynolds number, this should imply that the outer structure in the outer coordinate should extend more to the wall with the increase of the Reynolds number, resulting in a feature which would be difficult to explain if the large-scale structure scales only in the outer unit.

To be more precise, we show the streamwise wave-number spectra of the streamwise velocity of turbulent channel flow in Fig. 1. Here, the data are taken from previous direct numerical simulations at  $\text{Re}_\tau = 934, 2003, 5186$  [3,19] where  $\text{Re}_\tau = u_\tau h/\nu$  ( $u_\tau$  is the friction velocity,  $\nu$  is the kinematic viscosity, and  $h$  is the half-height of the channel). Figures 1(a) and 1(b) show the inner- and outer-scaled spectra, respectively. Not surprisingly, the spectra exhibit very good inner-scaling behavior in the near-wall region with the inner peak at  $\lambda_x^+ \simeq 1000$  [Fig. 1(a); here  $\lambda_x$  is the streamwise wavelength]. The energetic part of the spectra exhibits a linear growth with  $y$  along the ridge  $\lambda_x \simeq 100y$  ( $y$  is the wall-normal distance from the wall) on increasing the Reynolds number, indicating the emergence of the self-similar streaky motion in the logarithmic region found in Ref. [20]. However, the good inner scaling of the spectra is limited only for  $\lambda_x^+ \lesssim O(10^3)$  even in the near-wall region: The spectra for  $\lambda_x^+ \gtrsim O(10^4)$  in the region of  $y^+ \lesssim 50$  become increasingly more energetic and extend to the longer streamwise wavelengths on increasing the Reynolds number [the blue-boxed region in Fig. 1(a)], indicating the near-wall influence of the energy-containing motions in the logarithmic and outer regions at higher Reynolds numbers. This feature is also confirmed in the outer-scaled spectra [Fig. 1(b)]. The outer-scaled spectra appear to scale very well in the outer unit for  $\lambda_x > 1h$  and  $y > 0.2-0.3h$ , the spectral region to which large-scale motions (LSMs) and VLSMs would dominantly contribute. The most energetic part of the spectra gradually extends to the wall along the linear ridge  $\lambda_x \simeq 100y$  on increasing the Reynolds number. However, this extension is not limited only along  $\lambda_x \simeq 100y$ : The part of the spectra at  $\lambda_x \simeq 10-20h$  also appears to extend to the wall as the Reynolds number increases [the blue-boxed region in Fig. 1(b)]. This observation clearly confirms that the near-wall part (i.e., footprint) of the large-scale outer structure does not scale in the outer unit and that it extends more to the wall on increasing the Reynolds number.

Given the wall-normal location of the footprint of the large-scale outer structure, the only relevant length scale for its proper scaling would now be the inner length scale. The streamwise wave-number

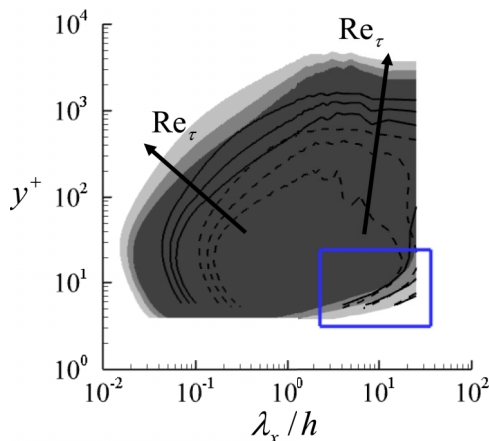


FIG. 2. Premultiplied streamwise wave-number spectra of the streamwise velocity in  $\lambda_x/h - y^+$  plane. The labels of each contour are given to be uniformly spaced from zero for comparison of the wall-normal structure of the spectra in the region highlighted with the blue box. Here, the dashed, solid, and shaded contours are respectively from  $Re_\tau = 934$ ,  $Re_\tau = 2003$  [19], and  $Re_\tau = 5186$  [3].

spectra of the streamwise velocity are therefore replotted in the  $\lambda_x/h - y^+$  plane in Fig. 2. Here, we note that the contour labels of the spectra at each different Reynolds number in Fig. 2 are chosen to be spaced uniformly from zero to make comparison of the structure of the spectra at  $\lambda_x \simeq 10\text{--}20h$  in the near-wall region. Figure 2 now reveals that the wall-normal structure of the streamwise velocity spectra at  $\lambda_x \simeq 10\text{--}20h$  in the near-wall region scales quite well in the inner unit (the blue-boxed region in Fig. 2), indicating that the near-wall part of the large-scale outer structures is dominated by viscous effect of the wall. From the scaling viewpoint, this observation turns out to be very important, as it would indicate that the wall-normal location of the outer peak in the streamwise wave-number spectra of the streamwise velocity should be the outcome of an asymptotic matching between two functions, one of which scales in the inner unit in the near-wall region and the other scales in the outer unit in the outer region, resulting in the Reynolds-number-dependent behavior of the outer peak.

The observation for the large-scale outer structure is remarkably similar to the concept of the mesolayer introduced for momentum balance of mean velocity (e.g., Ref. [12]), yielding several important questions: What is the origin of the inner-scaling nature of the large-scale outer structure in the near-wall region? Can this behavior also be observed in the self-similar energy-containing motions in the form of Townsend's attached eddies mainly populating the logarithmic region [20–22]? What is its consequence in relation to the classical theory of Ref. [21]? Does this behavior also appear in other variables such as wall-normal and spanwise velocities? The goal of the present study is to explore these issues. To this end, we first introduce a linear theory used in our previous studies in Sec. II [23–27], where optimal transient growth of small organised perturbations is computed using the linearized Navier-Stokes equation with an appropriate eddy viscosity [28]. In Sec. III, we show that the most amplified mode in the linear theory exhibits the qualitatively same behavior with the spectra in Figs. 1 and 2. Generalization of this observation is then made to the modes emerging in the form of Townsend's attached eddies in the logarithmic region [26], revealing that these modes also exhibits theoretically broken geometrical self-similarity due to their inner-scaling nature in the region close to the wall. In Sec. IV, the origin of this behavior is investigated with the linearized Navier-Stokes equation. A further discussion is given for other velocity components and Reynolds stress with direct numerical simulation (DNS) data available and with the statistics of the self-sustaining attached eddies in Ref. [20]. A summary and some remarks are given in Sec. V.

## II. LINEAR MODEL

### A. Linearized equation for a small-amplitude motion of interest

We consider a fluid flow over a turbulent channel in which the streamwise, wall-normal, and spanwise directions are denoted by  $x$ ,  $y$ , and  $z$ , respectively. The two walls are respectively located in  $y = 0$  and  $y = 2h$ . Density and kinematic viscosity of the fluid are denoted by  $\rho$  and  $\nu$ . The velocity field in the channel is denoted by  $\mathbf{u} = (u, v, w)$  where  $u$ ,  $v$ , and  $w$  indicate the streamwise, wall-normal, and spanwise velocities, respectively. Following Ref. [28], the velocity field  $\mathbf{u}$  may be decomposed as

$$\mathbf{u} = \mathbf{U} + \mathbf{u}' + \tilde{\mathbf{u}}, \quad (1)$$

where  $\mathbf{U} = (U(y), 0, 0)$  is the mean velocity,  $\mathbf{u}'$  is turbulent velocity fluctuation, and  $\tilde{\mathbf{u}}$  is the organized wave of interest. Here, it should be mentioned that the term *organized wave* is not meant to be the same as the commonly-used term *coherent structure*, which describes an ordered motion naturally emerging in a turbulent flow field. Instead, the velocity field  $\tilde{\mathbf{u}}$  rather represents a systematically controllable and/or tractable motion, which can be mathematically captured by an ensemble average. In this sense,  $\tilde{\mathbf{u}}$  is rather close to a perturbation in stability analysis of a laminar flow, often implemented in an organized or controlled manner through, e.g., vibrating ribbons [28].

If the amplitude of  $\tilde{\mathbf{u}}$  is small and an appropriate closure is provided for describing the role of  $\mathbf{u}'$  in evolution of  $\tilde{\mathbf{u}}$ , the equation for  $\tilde{\mathbf{u}}$  is given by

$$\nabla \cdot \tilde{\mathbf{u}} = 0, \quad (2a)$$

$$\frac{\partial \tilde{\mathbf{u}}}{\partial t} + (\tilde{\mathbf{u}} \cdot \nabla)\mathbf{U} + (\mathbf{U} \cdot \nabla)\tilde{\mathbf{u}} = -\frac{1}{\rho}\nabla\tilde{p} + \nabla \cdot [(v + \nu_t)(\nabla\tilde{\mathbf{u}} + \nabla\tilde{\mathbf{u}}^T)], \quad (2b)$$

with the initial condition

$$\tilde{\mathbf{u}}(x, y, z, t = 0) = \tilde{\mathbf{u}}_0(x, y, z). \quad (2c)$$

Here,  $\tilde{p}$  is the related pressure and  $\nu_t$  is the eddy viscosity. As in many previous studies [24,26,29,30], the semi-empirical expression in Ref. [31] is adopted for  $\nu_t$ :

$$\nu_t(\eta) = \frac{\nu}{2} \left( 1 + \frac{\kappa^2 \text{Re}_\tau^2}{9} (1 - \eta^2)^2 (1 + 2\eta^2)^2 \times \{1 - \exp[-(|\eta| - 1)\text{Re}_\tau/A]\}^2 \right)^{1/2} - \frac{\nu}{2}, \quad (3)$$

where  $\eta = (y - 1)/h$ ,  $\kappa = 0.426$ , and  $A = 25.4$  from Ref. [30]. Here, the given coefficients  $\kappa$  and  $A$  are tuned to have good agreement with the DNS data at  $\text{Re}_\tau \simeq 2000$  [30], and this analytically given profile enables us to perform the present analysis up to a very high Reynolds number ( $\text{Re}_\tau = 40\,000$ ) without suffering from the lack of the mean-velocity-profile measurement. Finally, it should be noted that the eddy viscosity here also has a direct relation with the mean velocity profile  $U(y)$  through the mixing length model, i.e.,  $\nu_t dU/dy = -\overline{u'v'}$ . This form of the eddy viscosity is obviously very crude and simple, but it contains a very important physical feature as discussed in detail in Sec. IV A.

### B. Optimal transient growth

Now, we consider a plane Fourier mode such that  $\tilde{\mathbf{u}}(x, y, z, t) = \hat{\mathbf{u}}(y, t)e^{i(\alpha x + \beta z)}$ , where  $\alpha$  and  $\beta$  are the streamwise and spanwise wave numbers, respectively (i.e.,  $\alpha = 2\pi/\lambda_x$  and  $\beta = 2\pi/\lambda_z$ ). It is instructive to use the normal velocity and vorticity form of the resulting equation [23,24]:

$$\frac{\partial}{\partial t} \begin{bmatrix} \hat{v} \\ \hat{\omega}_y \end{bmatrix} = \underbrace{\begin{bmatrix} \Delta^{-1} \mathcal{L}_{OS} & 0 \\ -i\beta U' & \mathcal{L}_{SQ} \end{bmatrix}}_A \begin{bmatrix} \hat{v} \\ \hat{\omega}_y \end{bmatrix}, \quad (4a)$$

where

$$\mathcal{L}_{OS} = -i\alpha(U\Delta - U'') + \nu_T\Delta^2 + 2\nu_T'\Delta\mathcal{D} + \nu_T''(\mathcal{D}^2 + k^2), \quad (4b)$$

$$\mathcal{L}_{SQ} = -i\alpha U + \nu_T\Delta + \nu_T'\mathcal{D}. \quad (4c)$$

Here,  $\hat{\omega}_y$  is the wall-normal vorticity of  $\hat{\mathbf{u}}(y,t)$ ,  $\nu_T = \nu + \nu_t$ ,  $\Delta = \mathcal{D}^2 - k^2$ ,  $k^2 = \alpha^2 + \beta^2$ , and  $\mathcal{D}$  and  $'$  denote  $\partial/\partial y$ .

The linear operator  $\mathbf{A}$  has been found to be stable in all the canonical wall-bounded shear flows considered so far [23–27]. Therefore, the amplification mechanism born by  $\mathbf{A}$  has been examined by computing its optimal response to given initial condition (optimal transient growth) [23–25,27] and/or given (harmonic or stochastic) body forcing [25–27]. For a given set of  $\alpha$  and  $\beta$ , the related optimization problem for initial condition is defined by

$$G_{\max} = \max_t \max_{\hat{\mathbf{u}}_0} \frac{\|\hat{\mathbf{u}}(t)\|^2}{\|\hat{\mathbf{u}}_0\|^2}. \quad (5)$$

Here, we note that  $\hat{\mathbf{u}}(t) = e^{t\mathbf{A}}\hat{\mathbf{u}}_0$ . Therefore,  $G_{\max}$  is nothing more than the square of two norms of the state transition operator  $e^{t\mathbf{A}}$  at  $t = t_{\max}$ , at which the largest amplification of  $\hat{\mathbf{u}}(t)$  is attained. In this respect, the optimization problem could be viewed as a tool to quantify the response of the linear operator  $\mathbf{A}$ . Such an optimization problem has recently been extended to incorporate the entire flow domain and/or nonlinearity to study transition, e.g., Refs. [32,33].

In the present study, the optimization problem is solved using the numerical solver successfully implemented for previous studies [23–25,27]. This solver projects  $\hat{\mathbf{u}}(t)$  onto the eigenspace of  $\mathbf{A}$ , and computes the solution of the optimization problem (5) using power iteration, which results in much faster calculation of the solution than the standard singular value decomposition. The discretization in the wall-normal direction is performed using a Chebyshev collocation method [34] with up to  $N_y = 1024$  to manage the highest Reynolds number considered here ( $\text{Re}_\tau = 40\,000$ ). For further details on the numerical method, the reader may refer to Ref. [35]. Since an extensive discussion on  $G_{\max}$  was made in Refs. [24,26], the focus on the present study will be given to the wall-normal structure of  $\hat{\mathbf{u}}_{\text{opt}}$  at  $t = t_{\max}$ , which represents the most amplified flow structure by (2), in relation to its similarity to the observation made with the spectra (Figs. 1 and 2).

### C. Relevance and limitations

Before exploiting the result from the present linear approach, here we address the physical relevance and limitations of the present approach based on a linear operator with a very crude eddy viscosity. The linear theory in the present study has been found to be useful for prediction of the generation of the long streaky structures emerging in the near-wall, logarithmic, and outer regions [23–27]. Large amplification of  $\hat{\mathbf{u}}$  appears typically for  $\alpha \ll \beta$ , and the resulting velocity field  $\hat{\mathbf{u}}_{\text{opt}}$  is dominated by a streaky motion of the streamwise velocity. This large amplification of the streamwise velocity essentially originates from the off-diagonal term  $-i\beta U'$  in Eq. (4), which represents tilting of the streamwise vorticity by the mean shear (i.e., lift-up effect). It is also important to mention that this term has the same mathematical origin with turbulence production term in the standard budget analysis and is the leading source of the non-normal nature of  $\mathbf{A}$  yielding large  $G_{\max}$  [35]. Indeed, in full simulations, the artificial inhibition of this term has been shown to destroy the large amplification of the long streamwise velocity structure (i.e., streak) as well as the related self-sustaining process of the energy-containing motions at all the length scales (i.e., inner, log-layer, and outer length scales) [36,37].

Despite the important predictions of the present linear theory, it has some important limitations. Not surprisingly, the main limitation is the linear nature. However, this appears in a more structured manner and becomes particularly crucial if the wall-normal and spanwise velocities are concerned. In real flow, the main flow structures of these velocity components are typically much shorter than the long streaky structure of the streamwise velocity: The streamwise extent of the flow structure with

the intense cross-streamwise velocity fluctuations is only two or three times larger than its spanwise width ( $\lambda_x \simeq 2-3\lambda_z$ ), whereas the streaky structure of the streamwise velocity appears with ten times larger than that ( $\lambda_x \simeq 10\lambda_z$ ) [20,38]. Given the fact that the linear amplification is large only for  $\alpha \ll \beta$ , it is questionable whether the linear theory would be fully relevant for such a short structure. Indeed, it has recently been shown that the length scale of the cross-streamwise velocity components is rather well predicted by instability of the amplified streaky structure, which incorporates some roles of the neglected nonlinearity [39–41]. A recent numerical experiment further confirmed this by showing that the artificial suppression of the instability of the amplified streak significantly inhibits the generation of the flow structure with the cross-streamwise velocity components [37].

The introduction of the eddy viscosity in Eq. (2) also needs to be discussed. The use of  $\nu_t$  with the linearized equation implicitly assumes that the perturbed motion of interest  $\tilde{\mathbf{u}}$  would feel the effect of surrounding turbulence in the same way that the mean flow does, given the fact that  $\nu_t$  is obtained from the mean flow with Prandtl’s mixing length model. It is therefore reasonable to expect that (2) would only be useful to describe the evolution of the motions, the time scale of which is much larger than or at least is at the order of the time scale of the mean shear [i.e.,  $O(1/S)$  where  $S \sim O(dU/dy)$ ] [28]. In this respect, (2) shares some important similarities to the rapid distortion theory, which relies on the linearized equation without  $\nu_t$  (e.g., Ref. [42]): The rapid distortion theory is also built upon the assumption that the characteristic time scale of the structure of interest to be much larger than  $O(1/S)$ . Reference [43] recently pointed out that the energy-containing motions in the logarithmic region and a certain part of the outer region ( $y/h < 0.5$ ) may be this case, as their time scale is about ten times larger than  $1/S$ . Clearly, the two different theoretical frameworks have similar working conditions. However, the presence of the eddy viscosity makes the outcomes of the two theories not exactly identical, as we shall see in Sec. IV A, where the presence of  $\nu_t$  is shown to play a crucial role in making  $\tilde{\mathbf{u}}$  behave as in the spectra in Figs. 1 and 2.

### III. RESULT

Throughout the present study, we will consider the spanwise wavelength  $\lambda_z$  between  $\lambda_z^+ = 100$  and  $\lambda_z = 1.5h$ . For each  $\lambda_z$ , the streamwise extent of the streaky motions is chosen to be

$$\lambda_x \simeq 10\lambda_z, \quad (6)$$

following our recent work in which the self-sustaining energy-containing motions were shown to exist in the form of Townsend’s attached eddies [20]. We note that if  $\lambda_z^+ = 100$ , (6) gives  $\lambda_x^+ = 1000$ , resulting in the streamwise length scale of the near-wall streaks. On the other hand, if  $\lambda_z = 1.5h$ , it leads to  $\lambda_x = 15h$  which represents the streamwise length scale of the VLSM (the outer streaky structure). Each of the intermediate spanwise length scales  $\lambda_z$  between  $\lambda_z^+ = 100$  and  $\lambda_z = 1.5h$  yields the streamwise length scale of the self-similar streaky motions populating mainly the logarithmic region in the sense that their size is proportional to the distance from the wall. For a further discussion on (6), the reader may refer to Ref. [20]. Finally, it should be mentioned that the result presented in this section does not qualitatively depend upon the choice of the wavelengths as long as  $\lambda_x$  is chosen to be much larger than  $\lambda_z$  (see also Refs. [24,26] for further details).

#### A. Largest attached eddy: very-large-scale motion

We first consider  $\lambda_z = 1.5h$  with  $\lambda_x = 15h$  from (6), and this set of the wavelengths would represent the VLSM (the outer streaky structure) [20,38]. Figure 3 shows the wall-normal profiles of the normalized  $\hat{u}_{\text{opt}}$  for  $\text{Re}_\tau = 1000, 2000, 5000, 10\,000, 20\,000, 40\,000$ . If the profiles are plotted in the outer coordinate [Fig. 3(a)], they show good agreement with one another for  $y/h \gtrsim 0.2-0.3$ . However, they do not show such an agreement in the region close to the wall ( $y/h \lesssim 10^{-2}$ ): The normalized  $\hat{u}_{\text{opt}}$  rather tends to gradually extend to the wall on increasing the Reynolds number, similarly to the spectra at  $\lambda_x \simeq 10-20h$  [Fig. 1(a)]. Now, we normalize the profiles with their shear rate at the wall (i.e.,  $d\hat{u}_{\text{opt}}/dy^+|_{y=0}$ ) and plot them in the inner coordinate [Fig. 3(b)]. The rescaled

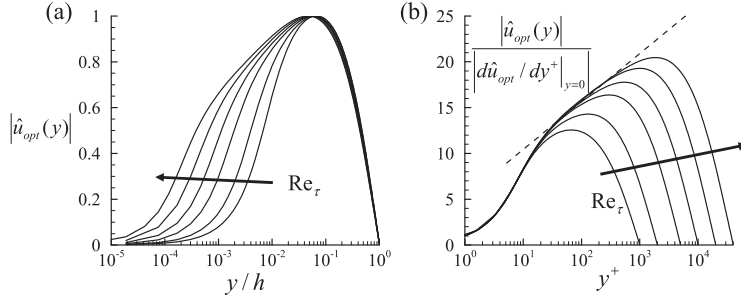


FIG. 3. The wall-normal profile of the normalized streamwise velocity of  $\hat{\mathbf{u}}_{\text{opt}}$  ( $\lambda_x = 15h$  and  $\lambda_z = 1.5h$ ): (a)  $|\hat{u}_{\text{opt}}(y/h)|$ ; (b)  $|\hat{u}_{\text{opt}}(y^+)|/|d\hat{u}_{\text{opt}}/dy^+|_{y=0}$ . Here,  $\text{Re}_\tau = 1000, 2000, 5000, 10\,000, 20\,000, 40\,000$ . The dashed line indicates  $|\hat{u}_{\text{opt}}(y^+)| = 1/0.44\ln(y^+) + 5.2$ .

profiles then reveal to scale very well in the inner coordinate. For relatively low Reynolds numbers ( $\text{Re}_\tau = 1000, 2000, 5000$ ), the inner-scale profiles show good agreement up to  $y^+ \simeq 10\text{--}20$ , similarly to the streamwise wave-number spectra of the streamwise velocity at  $\lambda_x \simeq 10\text{--}20h$  (see Fig. 2). For the two highest Reynolds numbers considered ( $\text{Re}_\tau = 20\,000, 40\,000$ ), the collapse reaches even up to  $y^+ \simeq 400$ , indicating that this behavior is not simply limited to the near-wall region and may extend to the region much further from the wall at very high Reynolds numbers. This inner-scaling behavior of  $\hat{u}_{\text{opt}}$  was first originally pointed out in Refs. [23,26], but it had received very little attention due to the lack of any compelling evidence. With the spectra given in Fig. 2, we now clearly show that this is a behavior consistent with scaling of the large-scale outer structures in real flow.

Figure 3 indicates that  $\hat{u}_{\text{opt}}(y)$  is a function of only  $y/h$  in the outer region [Fig. 3(a)], whereas  $\hat{u}_{\text{opt}}(y)/(d\hat{u}_{\text{opt}}/dy^+|_{y=0})$  is a function of only  $y^+$  in the near-wall region [Fig. 3(b)]. It is apparent that this feature would lead the peak location of  $\hat{u}_{\text{opt}}(y)$  (denoted by  $y_{\text{max}}$ ) to be placed in the overlap region with a scaling behavior involving both the inner and outer length scales. Such a scaling nature of  $\hat{u}_{\text{opt}}(y)$  is also an analog to the construction of the mean velocity (e.g., Refs. [44,45]), and the logarithmic behavior seems to emerge in  $\hat{u}_{\text{opt}}(y)$  in the same manner. In this respect, it is worth mentioning that Ref. [22] imposed a similar logarithmic dependence of the wall-normal structure to their statistical model of each attached eddy. Interestingly, in the present linear theory, such an logarithmic dependence naturally emerges in  $\hat{u}_{\text{opt}}(y)$  without such an imposition.

The peak location  $y_{\text{max}}$  with the Reynolds number is reported in Fig. 4. The peak location  $y_{\text{max}}$  in the outer coordinate gradually moves towards the wall on increasing the Reynolds number [Fig. 4(a)], whereas it gradually moves further from the wall in the inner coordinate with the Reynolds number

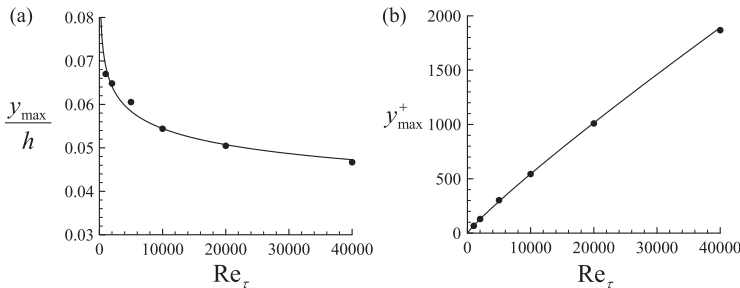


FIG. 4. Wall-normal peak location of the streamwise velocity of the optimal response at  $t = t_{\text{max}}$  with respect to  $\text{Re}_\tau$ . Here, the solid lines in panels (a) and (b) respectively indicate  $y/h = c\text{Re}_\tau^{-0.1019}$  and  $y^+ = c\text{Re}_\tau^{0.8981}$ , where  $c$  is a fitting constant.

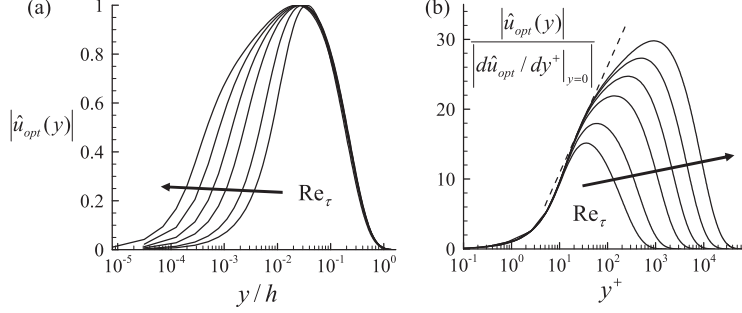


FIG. 5. The wall-normal profile of the normalized streamwise velocity of  $\hat{\mathbf{u}}_{\text{opt}}$  ( $\lambda_x = 6h$  and  $\lambda_z = 0.6h$ ): (a)  $|\hat{u}_{\text{opt}}(y/h)|$ ; (b)  $|\hat{u}_{\text{opt}}(y^+)|/|d\hat{u}_{\text{opt}}/dy^+|_{y=0}$ . Here,  $\text{Re}_\tau = 1000, 2000, 5000, 10\,000, 20\,000, 40\,000$ . The dashed line indicates  $|\hat{u}_{\text{opt}}(y^+)| = 1/0.15 \ln(y^+) - 4.5$ .

[Fig. 4(b)]. The best fit to the dependence of  $y_{\text{max}}$  on  $\text{Re}_\tau$  is found to be  $y/h \sim \text{Re}_\tau^{-0.1019}$  with the data available up to  $\text{Re}_\tau = 40\,000$ . The scaling of  $y_{\text{max}}$  is apparently not very close to  $y/h \sim \text{Re}_\tau^{-0.5}$  observed in boundary layer and pipe flows [4,6], although qualitatively the same trend is maintained. However, this is not so surprising, given the very crude nature of the present approach: The structure of  $\hat{u}_{\text{opt}}(y)$  is only an outcome of a linear theory given with inaccurate mean-velocity profiles (i.e., Cess profile), highly simplified eddy viscosity, and an initial condition obtained only by solving an optimization problem (6). In this respect, the characteristics of  $\hat{u}_{\text{opt}}(y)$  and  $y_{\text{max}}$  with  $\text{Re}_\tau$  in Figs. 3 and 4 is rather quite encouraging, as they exhibit qualitatively the same physical behavior with the spectra in Figs. 1 and 2.

### B. Attached eddies in the logarithmic region

Now, we extend our investigation on  $\hat{u}_{\text{opt}}(y)$  to the logarithmic region by considering  $\lambda_z$  between  $\lambda_z^+ = 100$  and  $\lambda_z = 1.5h$ , as a spanwise length scale in this range would describe each of the self-similar streaky structures in the logarithmic region [20,37]. We first choose  $\lambda_z$  so that it scales in the outer unit. Figure 5 shows the wall-normal profiles of  $\hat{u}_{\text{opt}}(y)$  at  $\lambda_z = 0.6h$  with  $\lambda_x = 6h$  for  $\text{Re}_\tau = 1000, 2000, 5000, 10\,000, 20\,000, 40\,000$ . Exactly the same behavior is observed as in Fig. 3. When plotted in the outer coordinate, the normalized profiles of  $\hat{u}_{\text{opt}}(y)$  at the different Reynolds numbers agree well with one another for  $y/h > 0.03 \sim 0.04h$  [Fig. 5(a)]. On the other hand, when plotted in the inner coordinate, the profiles normalized with their respective gradient at the wall collapses well with one another in the region relatively close to the wall [Fig. 5(b)]. The logarithmic dependence of  $\hat{u}_{\text{opt}}(y)$  is also seen, although the wall-normal size of the related region appears to be much smaller than that with  $\lambda_z = 1.5h$  (Fig. 3) due to the smaller  $\lambda_z (=0.6h)$  in this case. Here, it should be noted that there is no reason for  $\hat{u}_{\text{opt}}(y)$  to have the same coefficient for the logarithmic dependence as the Kármán constant, as its outer profile is completely different from that of the mean velocity.

We now choose  $\lambda_z$  so that it scales in the inner unit with the Reynolds number. In this case, the behavior in Figs. 3 and 5 turns out to be quite different. Figure 6 shows the normalized  $\hat{u}_{\text{opt}}(y)$  in the inner coordinate for  $\lambda_z^+ = 100$  and  $\lambda_z^+ = 300$  at  $\text{Re}_\tau = 1000, 2000, 5000, 10\,000, 20\,000, 40\,000$ . Unlike Figs. 3 and 5, the profiles at all the Reynolds numbers considered are almost identical to one another in the inner coordinate. This suggests that the scaling of the outer part of  $\hat{u}_{\text{opt}}(y)$  essentially depends upon the choice of the scaling of  $\lambda_z$  (i.e., the size of the structure of interest). It is important to note that this feature is in contrast to the inner part of  $\hat{u}_{\text{opt}}(y)$ : Figures 4 and 5 suggest that no matter how  $\lambda_z$  is chosen, the inner part of  $\hat{u}_{\text{opt}}(y)$  always remains to scale in the inner unit.

In the previous study [26],  $\hat{u}_{\text{opt}}(y)$  for a given  $\lambda_z$  between  $\lambda_z^+ = 100$  and  $\lambda_z = 1.5h$  was found to be approximately self-similar with respect to  $\lambda_z$  or  $y$ , consistent with Townsend's attached eddy hypothesis [21]. Further to this previous finding, the observation given with Figs. 5 and 6 more

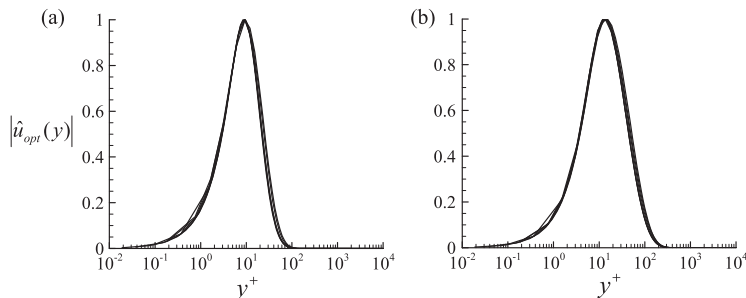


FIG. 6. Normalized streamwise velocity profile of the optimal response at  $t = t_{\max}$ : (a)  $\lambda_x^+ = 1000$  and  $\lambda_z^+ = 100$ ; (b)  $\lambda_x^+ = 3000$  and  $\lambda_z^+ = 300$ . Here,  $\text{Re}_\tau = 1000, 2000, 5000, 10\,000, 20\,000, 40\,000$ .

precisely suggests that the self-similar nature of  $\hat{u}_{\text{opt}}(y)$  would be valid only in the approximate sense, because the inner part of  $\hat{u}_{\text{opt}}(y)$  does not appear to be affected by the chosen  $\lambda_z$ . Figure 7(a) shows the wall-normal profiles of  $\hat{u}_{\text{opt}}$  for  $\lambda_z/h = 0.3, 0.6, 0.9$  at  $\text{Re}_\tau = 10\,000$  in the  $y/\lambda_z$  coordinate. It appears that only the outer part of  $\hat{u}_{\text{opt}}$  is self-similar in this coordinate. More precise scaling with the  $y/y_{\max}$  coordinate (from  $\lambda_z \sim y$ ), shown in Fig. 7(b), more clearly reveals that it is indeed only the outer part of  $\hat{u}_{\text{opt}}$ , which exhibits a precise self-similarity with respect to  $y_{\max}$ . On the contrary, the near-wall part of  $\hat{u}_{\text{opt}}$  does not show such a self-similarity due to its inner-scaling nature. Instead,  $\hat{u}_{\text{opt}}$  extends more to the wall, as the chosen  $\lambda_z$  increases (Fig. 7). It should be stressed that this so-called incomplete self-similarity of  $\hat{u}_{\text{opt}}$  essentially originates from the inner-scaling nature of the near-wall part of  $\hat{u}_{\text{opt}}$ . This implies that such an incomplete self-similarity of the energy-containing motions in the logarithmic region of a real flow may also be observed, as the spectra in Fig. 2 at least partially support this idea. This issue will be further discussed in Sec. IV B.

#### IV. DISCUSSION

Using the linear theory in Sec. II, we have proposed that the near-wall streamwise velocity of the energy-containing motions in the logarithmic and outer regions would exhibit the inner-scaling nature, while their respective outer part scales in the length scale posed. It is important to mention that the spectra of the streamwise velocity at least for  $\lambda_x \gtrsim O(h)$  appears to well support this idea (Figs. 1 and 2). Since the inner-scaling nature of a certain flow feature would indicate the viscous wall effect, this proposition sounds quite like that of the mesolayer for the mean velocity [8–12]. The evidence given here with the spectra from DNSs and the linear theory suggests that such a mesolayer-like behavior would also be likely to exist in each of the energy-containing motions in the logarithmic and outer regions given in the form of Townsend's attached eddies. It is presumable

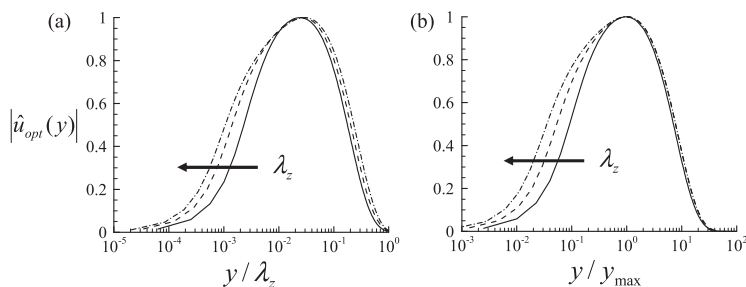


FIG. 7. Normalized streamwise velocity profile of the optimal response at  $t = t_{\max}$  ( $\text{Re}_\tau = 10\,000$ ) in (a) the  $y/\lambda_z$  and (b)  $y/y_{\max}$  coordinate. Here,  $\lambda_z/h = 0.3, 0.6, 0.9$ .

that this feature is intricately linked with the Reynolds-number-dependent behavior of the outer peak location in the streamwise wave-number spectra of the streamwise velocity [4,6] as well as higher-order statistics. In this respect, it is also worth mentioning a recent work [46], which showed that introducing a Reynolds-number-dependent spectral behavior to the wave numbers a little smaller than those for  $k_x^{-1}$  spectrum ( $k_x^{-1}$  is the streamwise wave number) improves the early spectral model of Ref. [47] physically with more consistent behavior. Here, we note that the wave-number range introduced in that work actually appears to describe the mesolayer-like behavior of the long streaky structures discussed here in the physical space, given its long wavelength (i.e., short wave number) and the Reynolds-number-dependent behavior.

It should also be mentioned that the observations in the present study are mainly on the coherent structures and the related spectra. However, this also appears to provide a consistent description for the recent work on the self-similar mean dynamics by Klewicki and coworkers [48,49]. These works have shown that the mean momentum equation admits an invariant form of the mean-momentum equation responsible for each of the wall-normal layers. The invariant form of the mean-momentum equation for each wall-normal layer is given in the same form of the original one for the entire wall-normal location [48,49]. It is important to note that the original mean-momentum equation itself contains a competitive dynamics between the inner and outer scales, typically featured with a four-layer structure. This implies that the same four-layer structure should appear in the mean-momentum equation for each wall-normal layer, indicating that this equation would also contain the influence of viscous scales in the presence of appropriate boundary conditions. This behavior is consistent with the present observation, but more rigorous mathematical treatments would be required in order to build more direct relation between the mean dynamics and the present observation.

Another important outcome of the presence of such a mesolayer-like structure in the energy-containing motions in the logarithmic and outer regions is that their self-similarity would be incomplete or at least partially broken in the region close to the wall due to the inner-scaling nature of each motion (Fig. 7). However, it should be pointed out that this feature is not necessarily inconsistent with the original theory [21], which posed the self-similarity of the energy-containing motions in the logarithmic region as the cornerstone. It is important to recall that the statistical structure of each attached eddy was originally constructed in the inviscid limit by neglecting the viscous effect from the wall. The reason that the incomplete self-similarity appears in the present study is essentially because this neglected viscous wall effect is incorporated in the structure of the attached eddies. In this respect, the incomplete self-similarity should be viewed as a consequence of viscous correction of the original description on the attached eddies. Finally, it should be mentioned that the incomplete self-similarity in the streamwise velocity does not necessarily affect description of the mean velocity profile, as the mean-velocity dynamics is only directly related with the Reynolds shear stress [48,49]. This is essentially because the incomplete self-similar part in the streamwise velocity emerges in the region close to the wall, where each of the energy-containing motions in the logarithmic and outer regions is supposed to carry very little Reynolds stress (i.e., inactive). Indeed, we will see that the incomplete self-similarity does not appear in the Reynolds shear stress (Sec. IV B).

Thus far, the focus of the present study has been given to our observation on the inner-scaling nature of the streamwise velocity of the energy-containing motions in the logarithmic and outer regions and its physical implications. The rest of this section will be devoted to understanding the origin of this behavior using the linear theory in Sec. II and the behavior of other variables such as wall-normal velocity, spanwise velocity, and Reynolds shear stress.

### A. The origin of the inner-scaling nature

A careful examination of the linear model in Sec. II reveals that the origin of the inner-scaling nature of  $\hat{u}_{\text{opt}}(y)$  is the eddy viscosity  $\nu_t$  given in the form of (3). Figure 8 compares the profile of  $\hat{u}_{\text{opt}}(y)$  for  $\lambda_z = 1.5h$  with the one recomputed by setting a constant eddy viscosity such that  $\nu_t = \max_y \nu_t(y)$  at  $\text{Re}_\tau = 10000$ . The original  $\hat{u}_{\text{opt}}(y)$  with  $\nu_t$  in Eq. (3) spreads over the entire

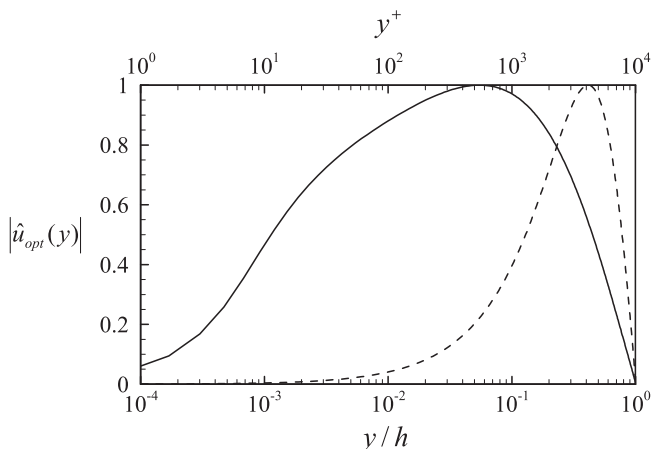


FIG. 8. Effect of the eddy viscosity on the normalized streamwise velocity profile of the optimal response at  $t = t_{\max}$  ( $\lambda_z = 1.5h$ ,  $\lambda_x = 15h$ , and  $\text{Re}_\tau = 10\,000$ ): the original eddy viscosity (solid line) and a constant eddy viscosity with  $\nu_t = \max_y \nu_t(y)$  (dashed line) where  $\nu_t(y)$  is given in Eq. (3).

wall-normal location and produces its  $y_{\max}$  in the logarithmic region ( $y_{\max}/h = 0.055$ ). On the other hand,  $\hat{u}_{\text{opt}}(y)$  with the constant  $\nu_t$  does not have appreciable amplitude below  $y^+ = 100$  ( $y/h = 0.01$ ) and its peak wall-normal location is placed at  $y_{\max} = 0.4h$  in the outer region. More importantly, if the original  $\nu_t$  is replaced by the constant  $\nu_t$ ,  $\hat{u}_{\text{opt}}(y)$  is found to depend very little on the Reynolds number as shown in Fig. 9. These observations clearly suggest that the spatially varying  $\nu_t$  given by (3) plays a key role in the large amplification of  $\hat{u}_{\text{opt}}(y)$  in the near-wall and logarithmic regions as well as the enforcement of the inner-scaling nature of  $\hat{u}_{\text{opt}}(y)$  in the region close to the wall.

The key feature of  $\nu_t$  in Eq. (3) essentially lies in its definition given by the mixing length model, i.e.,

$$\nu_t \frac{dU}{dy} = -\overline{u'v'}. \quad (7)$$

In the logarithmic region, the Reynolds stress has its maximum, but is roughly constant and  $dU/dy \sim 1/y$ . Therefore, the considered  $\nu_t$  should grow linearly with  $y$ . Here, it is very important to note that this growing behavior of  $\nu_t$  in the logarithmic region must be generic in any turbulence models for

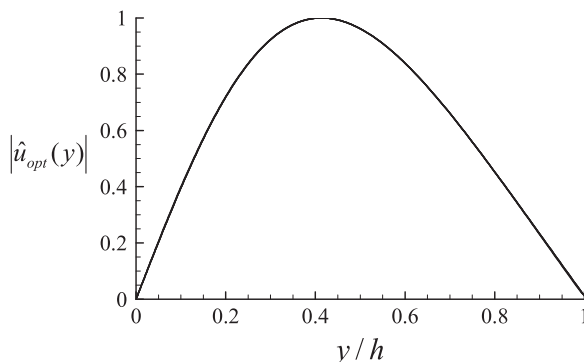


FIG. 9. Dependence on the normalized streamwise velocity profile of the optimal response at  $t = t_{\max}$  on the Reynolds number with a constant eddy viscosity  $\nu_t = \max_y \nu_t(y)$ . Here,  $\text{Re}_\tau = 1000, 2000, 5000, 10\,000, 20\,000, 40\,000$ . Note that all the profiles considered are almost identical.

wall-bounded shear flows. In the near-wall region, both the integral and dissipation length scales become identical to each other by being  $\delta_v$ , indicating that the dissipation mechanism would be dominated by molecular viscosity. On the other hand, in the outer region, the integral length scale ( $h$ ) exhibits large separation from the dissipation length scale ( $\nu^3 h / u_\tau^3$ ), the extent of which would be measured by their ratio given by  $\text{Re}_\tau^{3/4}$ . A vigorous turbulent dissipation through the energy cascade is therefore expected in the outer region, yielding large  $\nu_t$  from the modeling viewpoint. In the logarithmic region, the very different dissipation mechanism between the near-wall and outer regions should be smoothly connected, and the only way for this to be incorporated would be by having an increasing  $\nu_t$  with  $y$ , as in Eq. (7).

This growing feature of  $\nu_t$  in the logarithmic region appears to be the major player in determining the wall-normal structure of  $\hat{u}_{\text{opt}}(y)$  in the present linear approach. In the near-wall region and relatively lower part of the logarithmic region, the relatively small  $\nu_t$  enables the given initial perturbation to undergo large amplification, whereas in the relatively upper part of the logarithmic region and outer region, the large  $\nu_t$  does not allow it to be largely amplified. This simple mechanism explains why  $\hat{u}_{\text{opt}}(y)$  with  $\nu_t$  in Eq. (3) is larger than that with the constant  $\nu_t [= \max_y \nu_t(y)]$  in the region close to the wall, while being smaller in the region far from the wall. It is also presumable that such a nature of  $\nu_t$  in Eq. (3) enforces the inner-scaling behavior of  $\hat{u}_{\text{opt}}(y)$ , given its direct relationship to the mean velocity through (7).

This importance of  $\nu_t$  in dictating the wall-normal structure of  $\hat{u}_{\text{opt}}(y)$  suggests that the inner-scaling nature of  $\hat{u}_{\text{opt}}(y)$  or the presence of the mesolayer-like behavior of the energy-containing motions would probably be an outcome of a scale interaction, because the wall-normal structure of  $\nu_t$  in the present study essentially reflects the inhomogeneous turbulent dissipation affected by the multiple scales at different wall-normal locations. It is important to mention that this form of scale interaction, mimicked through  $\nu_t$  in the linear theory, is not only limited to the near-wall region, but also affects the evolution of a given motion of interest throughout the entire wall-normal location. This interpretation also allows us to distinguish the present linear theory from the rapid distortion theory: The former describes the evolution of the motions under the influence of minimal form of such a scale interaction (i.e., background turbulence), whereas the latter describes it in the absence of such a scale interaction. This interpretation appears to be consistent with Fig. 9, where the use of the constant  $\nu_t$  in the wall-normal direction is shown to yield  $\hat{u}_{\text{opt}}(y)$  scaling completely within the outer units.

## B. Other variables

Finally, the behavior of other variables, such as wall-normal velocity, spanwise velocity and Reynolds shear stress, is discussed. Figure 10 shows the streamwise wave-number spectra of the wall-normal velocity, the spanwise velocity, and the Reynolds shear stress. Due to relatively low Reynolds numbers considered here, the spectra do not very clearly show linearly growing nature with distance from the wall yet (i.e.,  $\lambda_x \sim y$ ), although this behavior begins to be apparent on increasing the Reynolds number. Therefore, the focus of this discussion will be given to the large-scale outer structures as in the introduction due to relatively small logarithmic region at low Reynolds numbers considered. However, it should be mentioned that the discussion can be further extended for the structures in the logarithmic region, if accurate near-wall spectra are available at much higher Reynolds number. In the near-wall region ( $y^+ < 50$ ), the spectra of the wall-normal velocity and the Reynolds shear stress show very good scaling in the inner unit [Figs. 10(a) and 10(e)]. However, these spectra do not extend to longer streamwise wavelengths in the near-wall region on increasing the Reynolds number [the boxed region in Figs. 10(a) and 10(e)], unlike those of the streamwise velocity [compare with Fig. 1(b)]. This feature is also confirmed in the outer-scaled spectra of these variables [Figs. 10(b) and 10(f)], which do not show any penetrating behavior of the motions for  $\lambda_x > O(h)$  into the near-wall region. This indicates that the wall-normal velocity component and the Reynolds shear stress of the motions in the logarithmic and outer regions may not exhibit the inner-scaling nature in the near-wall region, as they do not make any contribution to the near-wall region.

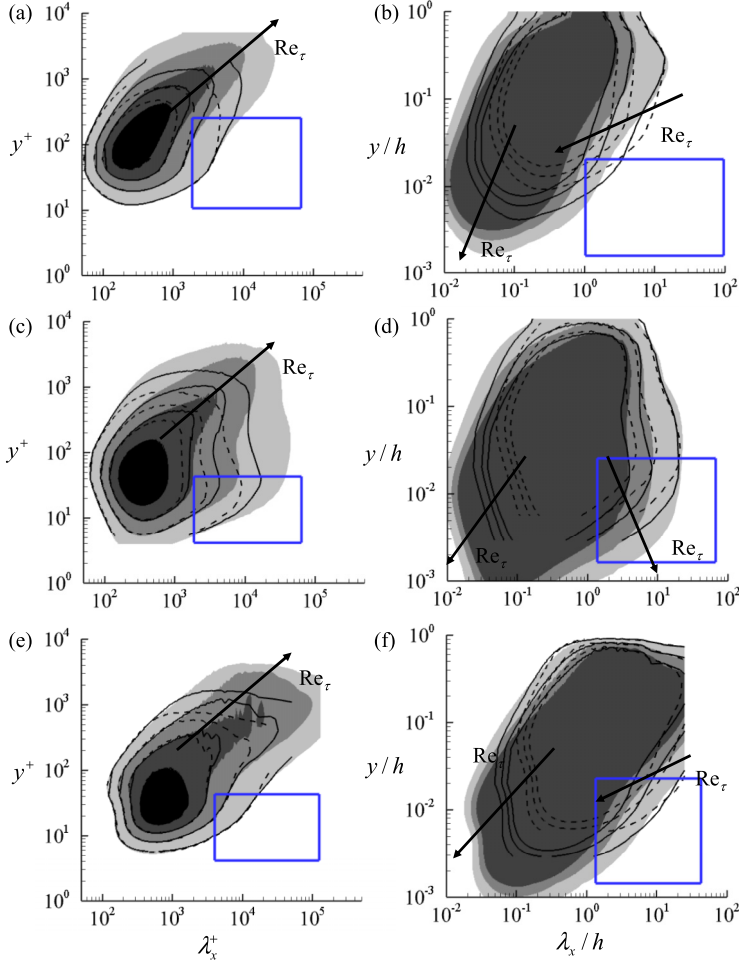


FIG. 10. Different scaling of the streamwise wave number spectra of (a), (b) wall-normal velocity, (c), (d) spanwise velocity, and (e), (f) Reynolds stress: (a), (c), (e) inner scaling in the  $\lambda_x^+$ - $y^+$  plane with the contour labels, 0.2, 0.4, 0.6, and 0.8 times of each maximum; (b), (d), (f) outer scaling in the  $\lambda_x/h$ - $y/h$  plane with the contour labels, 0.1, 0.2, and 0.3 times of each maximum. Here, the dashed, solid, and shaded contours are respectively from  $Re_\tau = 934$ ,  $Re_\tau = 2003$  [19], and  $Re_\tau = 5186$  [3]. In each of the subfigures, the region of interest is highlighted with a blue box.

On the contrary, the spectra of the spanwise velocity appear to behave very similarly to those of the streamwise velocity. In the near-wall region, the spectra of the spanwise velocity exhibit an extending behavior to longer streamwise wavelengths on increasing the Reynolds number, while revealing very good inner scaling only for  $\lambda_x^+ < O(10^3)$  [Fig. 10(c)]. Also, the outer-scaled spectra tend to extend more to the wall for  $\lambda_x > O(h)$  [Fig. 10(d)]. These behaviors are exactly the same as those observed for the streamwise velocity (compare with Figs. 1 and 2). This feature of the spanwise velocity further implies that the near-wall part of this velocity component for  $\lambda_x > O(h)$  would probably also scale well in the inner units, as indeed confirmed in Fig. 11 where the inner-scale nature of the near-wall streamwise wave-number spectra of the spanwise velocity is shown.

The emergence of the inner-scaling nature of the near-wall part of the spectra at  $\lambda_x > O(h)$  only in the streamwise and spanwise velocities suggests that the incomplete self-similarity of the energy-containing motions in the logarithmic region, pointed out in Sec. III B, would appear only

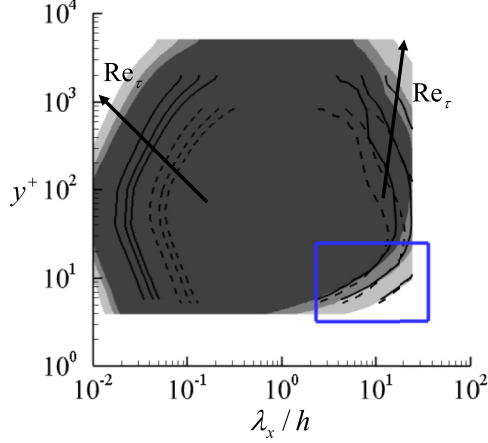


FIG. 11. Scaling of the streamwise wave number spectra of the spanwise velocity in the  $\lambda_x/h - y^+$  plane. The labels of each contour are uniformly spaced from zero. Here, the dashed, solid, and shaded contours are respectively from  $\text{Re}_\tau = 934$ ,  $\text{Re}_\tau = 2003$  [19], and  $\text{Re}_\tau = 5186$  [3]. The region of interest is highlighted with a blue box.

for their wall-parallel velocity components. To further investigate this issue, here we introduce the statistics of the energy-containing motions at a given  $\lambda_z$  (i.e., attached eddies) computed in Ref. [20], where these motions are found to be approximately self-similar with respect to the spanwise wavelength  $\lambda_z$ . The computation of such energy-containing motions in that study was carried out by physically removing all the motions except those at the given spanwise length scale using their self-sustaining nature [38,50,51]: The structures, the spanwise size of which is smaller than the given one, were artificially damped by artificially elevating the Smagorinsky constant of the large-eddy simulation using the static Smagorinsky model, while those larger than the given one were not resolved by imposing a restricted spanwise computational domains such that  $\lambda_z = L_z$  where  $L_z$  is the spanwise domain size. For further details, the reader may refer to Ref. [20].

Figure 12 shows the second-order statistics of the energy-containing motions in Ref. [20] for several  $\lambda_z$  with the logarithmic abscissa of the  $y/\lambda_z$ . As discussed in that work, the second-order statistics reveal approximately self-similar behavior for  $y/\lambda_z < 0.3-0.5h$  (note that the non-self-similar part at  $y/\lambda_z > 0.3-0.5h$  is an artifact of the numerical experiment; see Ref. [20] for a further discussion). Despite the very aggressive nature of the way of isolating the motions at a given  $\lambda_z$  in Ref. [20], it is interesting to note that the extent of the self-similarity of the wall-parallel velocity components [Figs. 12(a) and 12(c)] appears not to be better than that of the wall-normal velocity and Reynolds shear stress [Figs. 12(b) and 12(d)]. In particular, the wall-normal profiles of the streamwise and spanwise velocity fluctuations tend to penetrate deeper into the near-wall region, as  $\lambda_z^+$  is increased (compare also with Fig. 7), indicating that the self-similarity of these velocity components in the region close to the wall may be interpreted to be rather partially broken, consistent with the spectra in Figs. 2 and 11.

It should be mentioned that this interesting behavior is presumably linked to the nature of the eddy viscosity in the static Smagorinsky model used in Ref. [20], i.e.,

$$\nu_t = (C_s \tilde{\Delta})^2 \tilde{\mathcal{S}} \mathcal{D}, \quad (8)$$

where  $\tilde{\cdot}$  denotes the filtered quantity,  $C_s$  denotes the Smagorinsky constant,  $\tilde{\Delta}$  is the filter width given by the grid size,  $\tilde{\mathcal{S}} = (2\tilde{S}_{ij}\tilde{S}_{ij})^{1/2}$  is the norm of the strain rate tensor  $S_{ij}$ , and  $\mathcal{D} = 1 - \exp[-(y^+/A^+)^3]$  is the van Driest damping function with  $A^+ = 25$ . Here, the van Driest damping function  $\mathcal{D}$  indeed appears to enforce the eddy viscosity to behave like the one used in the linear theory, explaining the appearance of the broken self-similarity in the region close to the wall.

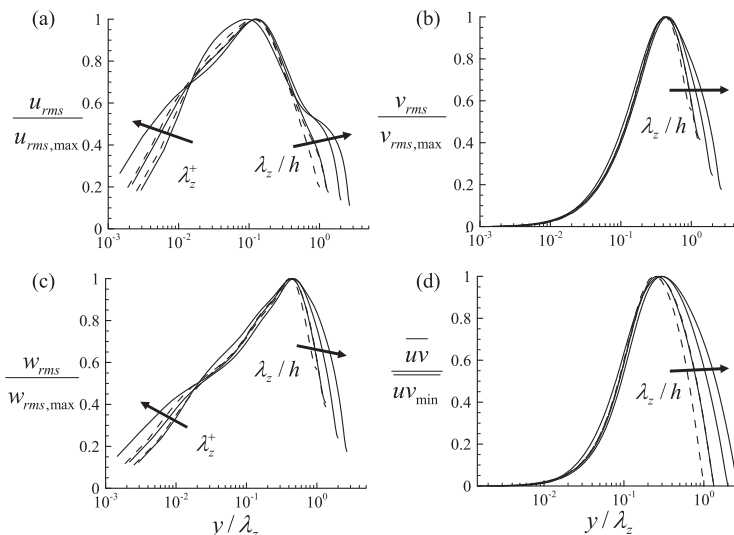


FIG. 12. Near-wall behavior of the second-order statistics of the self-sustaining attached eddies computed in Ref. [20]: (a) streamwise velocity; (b) wall-normal velocity; (c) spanwise velocity; (d) Reynolds stress. Here, the dashed lines denote  $\text{Re}_\tau \simeq 950$  ( $L950a$ ,  $L950b$ ) and the solid lines denote  $\text{Re}_\tau \simeq 1800$  ( $L1800a$ ,  $L1800b$ ,  $L1800c$ ) in Ref. [20].

However, it should be noted that the broken self-similarity in this case only dominantly appears in the wall-parallel velocity components, similarly to the inner-scaling nature of the spectra of real flows given in Figs. 2 and 11, even though they are enforced to all the velocity components. The only way to explain this behavior, observed consistently both in DNS and the numerical experiment in Ref. [20], would probably be that the inner-scaling nature (or the mesolayer-like structure) of the energy-containing motions in the logarithmic and outer regions is intricately linked with the boundary condition at the wall: The wall-normal velocity is not allowed to penetrate to the region close to the wall due to the impermeability component (i.e.,  $\partial v / \partial y = 0$  at the wall). In this respect, it would indeed be appropriate to interpret that this observation is a consequence of viscous correction of the attached hypothesis of Ref. [21], whose theory was originally built by neglecting the near-wall viscous effect to the attached eddies in the limit of very high Reynolds number.

## V. CONCLUDING REMARKS

The concept of the mesolayer has often been linked to the region affected by the viscous force originating from the presence of the wall in the mean momentum balance. The Reynolds number dependence of the peak wall-normal location of Reynolds shear stress has played a key role in defining the mesolayer [11,12,49]. The key finding in the present study with a linear theory and the DNS data available is that such viscous wall effect can exist in the wall-normal structure in all the energy-containing motions in the form of Townsend's attached eddies. In this sense, it would not be inappropriate to call the inner-scaling region of each of the energy-containing motions the mesolayer of the attached eddies. The consequence of applying the concept of the mesolayer to the attached eddy hypothesis [21] appears to be quite intriguing, as it allows one to have a consistent description of several important observations within a single framework, i.e., the viscous effect in the mean momentum balance [11,12,48,49], the near-wall penetration of the outer structures via their footprint resulting the inner-outer interaction [2,4,15–17], the Reynolds-number-dependent behavior of the outer peak in the streamwise wave-number spectra of the streamwise velocity [4,6], a viscous correction of Townsend's attached eddy hypothesis and the resulting incomplete self-similarity

in the region close to the wall (present study), and the collective generation of turbulent skin friction by all the energy-containing motions [18,52]. Incorporation of this observation to the early predictive models based on the attached eddy hypothesis would probably improve their capability (e.g., Refs. [22,46,47,53,54]), and it may be a fruitful way to follow towards a consistent statistical description of high-Reynolds-number wall turbulence.

#### ACKNOWLEDGMENTS

I am very grateful to Dr. M. K. Lee and Prof. R. D. Moser who kindly made their DNS data in public. This paper would not have been able to be written without their invaluable DNS data [3]. This work was supported by the Engineering and Physical Sciences Research Council (EPSRC) in the UK (EP/N019342/1).

- 
- [1] K. C. Kim and R. Adrian, Very large-scale motion in the outer layer, *Phys. Fluids* **11**, 417 (1999).
  - [2] N. Hutchins and I. Marusic, Evidence of very long meandering features in the logarithmic region of turbulent boundary layers, *J. Fluid Mech.* **579**, 1 (2007).
  - [3] M. K. Lee and R. D. Moser, Direct numerical simulation of the turbulent boundary layer over a cube-roughened wall, *J. Fluid Mech.* **774**, 395 (2015).
  - [4] R. Mathis, N. Hutchins, and I. Marusic, Large-scale amplitude modulation of the small-scale structures in turbulent boundary layers, *J. Fluid Mech.* **628**, 311 (2009).
  - [5] P. Vincenti, J. Klewicki, C. Morrill-Winter, C. M. White, and M. Wosnik, Streamwise velocity statistics in turbulent boundary layers that spatially develop to high Reynolds number, *Exp. Fluids* **54**, 1629 (2013).
  - [6] M. Vallikivi, B. Ganapathisubramani, and A. J. Smits, Spectral scaling in boundary layers and pipes at very high Reynolds numbers, *J. Fluid Mech.* **771**, 303 (2015).
  - [7] M. Hultmark, M. Vallikivi, S. C. C. Bailey, and A. J. Smits, Turbulent Pipe Flow at Extreme Reynolds Numbers, *Phys. Rev. Lett.* **108**, 094501 (2012).
  - [8] R. R. Long and T.-C. Chen, Experimental evidence for the existence of the mesolayer in turbulent systems, *J. Fluid Mech.* **105**, 19 (1981).
  - [9] N. Afzal, Fully developed turbulent flow in a pipe: An intermediate layer, *Ing.-Arch.* **52**, 355 (1982).
  - [10] N. Afzal, Mesolayer theory for turbulent flows, *AIAA J.* **22**, 437 (1984).
  - [11] K. R. Sreenivasan and A. Sahay, The persistence of viscous effects in the overlap region and the mean velocity in turbulent pipe and channel flows, in *Self-Sustaining Mechanisms of Wall Turbulence*, edited by R. Panton (Computational Mechanics Publications, Southampton, UK, 1997), pp. 253–272.
  - [12] T. Wei, P. Fife, J. C. Klewicki, and P. McMurtry, Properties of the mean momentum balance in turbulent boundary layer, pipe, and channel flows, *J. Fluid Mech.* **522**, 303 (2005).
  - [13] C. Morrill-Winter and J. C. Klewicki, Influences of boundary layer scale separation on the vorticity transport contribution to turbulent inertia, *Phys. Fluids* **25**, 015108 (2013).
  - [14] J. C. Klewicki, A description of turbulent wall-flow vorticity consistent with mean dynamics, *J. Fluid Mech.* **737**, 176 (2013).
  - [15] L. Agostini and M. Leschziner, On the influence of outer large-scale structures on near-wall turbulence in channel flow, *Phys. Fluids* **26**, 075107 (2014).
  - [16] L. Agostini and M. Leschziner, Predicting the response of small-scale near-wall turbulence to large-scale outer motions, *Phys. Fluids* **28**, 015107 (2016).
  - [17] J. Hwang, J. Lee, H. J. Sung, and T. A. Zaki, Inner-outer interactions of large-scale structures in turbulent channel flow, *J. Fluid Mech.* **790**, 128 (2016).
  - [18] Y. Hwang, Near-wall turbulent fluctuations in the absence of wide outer motions, *J. Fluid Mech.* **723**, 264 (2013).
  - [19] S. Hoyas and J. Jiménez, Scaling of the velocity fluctuations in turbulent channels up to  $Re_\tau = 2003$ , *Phys. Fluids* **18**, 011702 (2006).

- [20] Y. Hwang, Statistical structure of self-sustaining attached eddies in turbulent channel flow, *J. Fluid Mech.* **767**, 254 (2015).
- [21] A. A. Townsend, *The Structure of Turbulent Shear Flow* (Cambridge University Press, Cambridge, UK, 1976).
- [22] A. E. Perry and M. S. Chong, On the mechanism of turbulence, *J. Fluid Mech.* **119**, 173 (1982).
- [23] C. Cossu, G. Pujals, and S. Depardon, Optimal transient growth and very large scale structures in turbulent boundary layers, *J. Fluid Mech.* **619**, 79 (2009).
- [24] G. Pujals, M. García-Villalba, C. Cossu, and S. Depardon, A note on optimal transient growth in turbulent channel flows, *Phys. Fluids* **21**, 015109 (2009).
- [25] Y. Hwang and C. Cossu, Amplification of coherent streaks in the turbulent Couette flow: An input-output analysis at low Reynolds number, *J. Fluid Mech.* **643**, 333 (2010).
- [26] Y. Hwang and C. Cossu, Linear non-normal energy amplification of harmonic and stochastic forcing in the turbulent channel flow, *J. Fluid Mech.* **664**, 51 (2010).
- [27] A. P. Willis, Y. Hwang, and C. Cossu, Optimally amplified large-scale streaks and drag reduction in the turbulent pipe flow, *Phys. Rev. E* **82**, 036321 (2010).
- [28] W. C. Reynolds and A. K. M. F. Hussain, The mechanics of an organized wave in turbulent shear flow, part 3: Theoretical models and comparisons with experiments, *J. Fluid Mech.* **54**, 263 (1972).
- [29] K. M. Butler and B. F. Farrell, Optimal perturbations and streak spacing in wall-bounded turbulent shear flow, *Phys. Fluids* **5**, 774 (1993).
- [30] J. C. del Álamo and J. Jiménez, Linear energy amplification in turbulent channels, *J. Fluid Mech.* **559**, 205 (2006).
- [31] R. D. Cess, A survey of the literature on heat transfer in turbulent pipe flow, Westinghouse Research Rep. No. 8-0529-R24, 1958 (unpublished).
- [32] S. Cherubini, J.-C. Robinet, A. Bottaro, and P. De Palma, Optimal wave packets in a boundary layer and initial phases of a turbulent spot, *J. Fluid Mech.* **656**, 231 (2010).
- [33] S. M. E. Rabin, C. P. Caulfield, and R. R. Kerswell, Triggering turbulence efficiently in plane Couette flow, *J. Fluid Mech.* **712**, 244 (2012).
- [34] J. A. C. Weideman and S. C. Reddy, A MATLAB differentiation matrix suite, *ACM Trans. Math. Soft.* **26**, 465 (2000).
- [35] P. J. Schmid and D. S. Henningson, *Stability and Transition in Shear Flows* (Springer, New York, 2001).
- [36] J. Kim and J. Lim, A linear process in wall-bounded turbulent shear flows, *Phys. Fluids* **12**, 1885 (2000).
- [37] Y. Hwang and Y. Bengana, Self-sustaining process of minimal attached eddies in turbulent channel flow, *J. Fluid Mech.* **795**, 708 (2016).
- [38] Y. Hwang and C. Cossu, Self-Sustained Process at Large Scales in Turbulent Channel Flow, *Phys. Rev. Lett.* **105**, 044505 (2010).
- [39] W. Schoppa and F. Hussain, Coherent structure generation in near-wall turbulence, *J. Fluid Mech.* **453**, 57 (2002).
- [40] J. Park, Y. Hwang, and C. Cossu, On the stability of large-scale streaks in the turbulent Couette and Poiseuille flows, *C. R. Mécanique* **339**, 1 (2011).
- [41] F. Alizard, Linear stability of optimal streaks in the log-layer of turbulent channel flows, *Phys. Fluids* **27**, 105103 (2015).
- [42] S. B. Pope, *Turbulent Flows* (Cambridge University Press, Cambridge, UK, 2000).
- [43] J. Jiménez, How linear is wall-bounded turbulence, *Phys. Fluids* **25**, 110814 (2013).
- [44] C. B. Millikan, A critical discussion of turbulent flows in channels and circular tubes, in *Proceedings of the Fifth International Congress of Applied Mechanics* (John Wiley & Sons, New York, 1938).
- [45] H. Tennekes and J. L. Lumley, *A First Course in Turbulence* (MIT Press, Cambridge, MA, 1967).
- [46] J. C. Vassilicos, J.-P. Laval, J.-M. Foucaut, and M. Stanislas, The streamwise turbulence intensity in the intermediate layer of turbulent pipe flow, *J. Fluid Mech.* **774**, 324 (2015).
- [47] A. E. Perry, S. Henbest, and M. S. Chong, A theoretical and experimental study of wall turbulence, *J. Fluid Mech.* **165**, 163 (1986).
- [48] J. C. Klewicki, P. Fife, and T. Wei, On the logarithmic mean profile, *J. Fluid Mech.* **638**, 73 (2009).
- [49] J. C. Klewicki, Self-similar mean dynamics in turbulent wall flows, *J. Fluid Mech.* **718**, 596 (2013).

- [50] Y. Hwang and C. Cossu, Self-sustained processes in the logarithmic layer of turbulent channel flows, [Phys. Fluid](#) **23**, 061702 (2011).
- [51] S. Rawat, Y. Hwang, C. Cossu, and F. Rincon, On the self-sustained nature of large-scale motions in turbulent Couette flow, [J. Fluid Mech.](#) **782**, 515 (2015).
- [52] M. de Giovanetti, Y. Hwang, and H. Choi, Skin-friction generation by attached eddies in a turbulent channel, Proc. IUTAM (to be published).
- [53] A. E. Perry, J. D. Li, and I. Marusic, Towards a closure scheme for turbulent boundary layers using the attached eddy hypothesis, [Phil. Trans. R. Soc. London A](#) **336**, 67 (1991).
- [54] A. E. Perry and I. Marusic, A wall-wake model for the turbulence structure of boundary layers, part 1: Extension of the attached eddy hypothesis, [J. Fluid Mech.](#) **298**, 361 (1995).